Economic Optimisation of NBI and ECH Actuation in Fusion Reactors Using Simulated Annealing

Alexander Higginbottom

January 2025

Abstract

This study presents a one-dimensional radial plasma model optimised using simulated annealing to enhance the energy confinement time (τ_E) in tokamak fusion reactors. The decision process that led to the selection of simulated annealing, and the subsequent optimisation of this approach, is discussed. The model investigates the dependence of τ_E on Neutral Beam Injection (NBI) and Electron Cyclotron Heating (ECH) actuation, constrained by a total budget of $500 million. The optimal configuration achieved $\tau_E = 8.712$ s with $P_{\text{NBI}} = 19.37$ MW and $P_{\text{ECH}} = 34.0$ MW. These findings highlight the potential for optimised actuation strategies to significantly reduce operational costs while improving reactor performance, offering insights for fusion planning and accelerating the development of economically viable fusion energy systems.

1 Introduction and Background

As the world grapples with the escalating climate crisis, the role of fusion energy in contributing to a clean energy mix has become increasingly apparent. The scientific consensus is clear: to mitigate the worst impacts of climate change, greenhouse gas emissions must be drastically reduced, and carbon-free energy sources scaled up. The global temperature increase has already surpassed 1.5°C above pre-industrial levels, emphasizing the urgency of transitioning to sustainable energy systems. Following the Paris Climate Agreement's target of limiting global warming to below 2°C by 2100, it has been estimated that achieving this goal will require approximately 3% of global GDP by the year 2100 [1, 2]. Since the energy sector is responsible for 84% of global CO_2 emissions, investment in carbon-free energy solutions is indispensable.

Among these alternatives, fusion energy holds particular promise as a zero-emission energy source. Unlike wind and solar, which are intermittent and require large-scale energy storage, fusion could provide a stable and continuous supply of base-load power, fulfilling a similar role to fossil fuels in the current energy mix. By complementing renewable energy sources, fusion energy has the potential to play a critical role in the global transition to sustainable energy systems.

Tokamaks are the leading design for magnetic confinement fusion, offering a practical approach to harnessing the energy released in nuclear fusion reactions [4]. A tokamak confines plasma using a combination of toroidal and poloidal magnetic fields, creating a doughnut-shaped plasma where fusion reactions can occur. These devices aim to sustain high-temperature and high-density plasmas long enough to achieve net energy gain [5]. The International Thermonuclear Experimental Reactor (ITER), a multinational collaboration, represents the largest and most advanced tokamak experiment to date and is designed to demonstrate the feasibility of producing sustained fusion power at a scale relevant to future energy production. ITER serves as the inspiration for the parameters and design choices that shape the plasma model presented in this paper.

Fusion energy is derived from the process of nuclear fusion, in which light atomic nuclei combine to form heavier nuclei, releasing energy in accordance with Einstein's equation $E = mc^2$. For nearly a century, researchers have sought to replicate this process on Earth, inspired by the realization that the Sun and stars derive their energy from nuclear fusion. In controlled fusion experiments, achieving the conditions for sustained energy production requires overcoming numerous scientific and engineering challenges. Among these challenges, plasma confinement plays a central role [6].

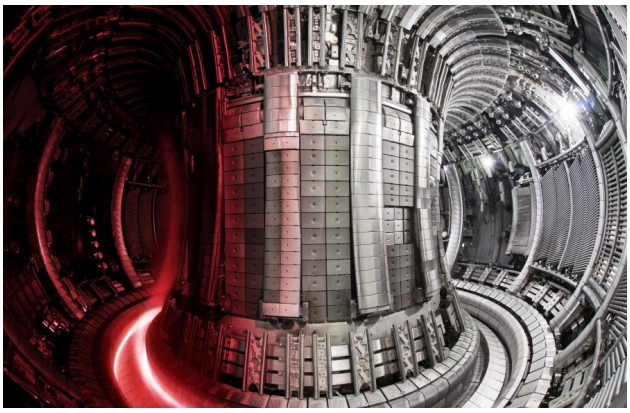

Figure 1: Inside JET (Joint European Torus) with plasmsa (left) and inactive (right), a formerly-functioning fusion reactor at UKAEA's Culham site [3].

When discussing fusion plasma physics, the single most important equation is the Lawson Criterion. It relates three critical parameters: the plasma temperature (T), the particle density (n), and the energy confinement time (τ). The criterion is typically expressed as:

$$nT\tau > \text{constant}, \tag{1}$$

where the constant depends on the type of fusion reaction [7]. For deuterium-tritium (D-T) fusion, the most common reaction under consideration, this constant is approximately 10^{21} keV·s·m^{-3} [8].

A key challenge for tokamak operation is optimizing the energy confinement time, τ, which quantifies how effectively the plasma retains its energy [9]. Plasma instabilities, transport losses, and interactions with the tokamak walls can degrade τ, making it a critical parameter for reactor performance. One of the key ways of stabilising the plasma and controlling the fusion reaction is by applying 'actuation' in the form of strong particle beams, most commonly Neutral Beam Injection (NBI) and Electron Cyclotron Heating (ECH). These systems are extremely costly, so careful design and preliminary modelling is essential.

In this work, we present a one-dimensional radial plasma model to simulate how τ varies with NBI and ECH actuation in a tokamak fusion reactor. By optimizing τ within cost constraints for NBI and ECH, we aim to provide insights into advancing tokamak performance and, ultimately, the development of economically viable fusion energy systems.

2 Methods

This section outlines the methodology employed in this study, focusing on two primary components: (i) constructing the model to represent the physical behavior of the tokamak plasma and (ii) setting up and performing the optimisation. Since the optimisation techniques described later assume a clear mathematical framework, this section aims to provide a detailed yet accessible description of the model, emphasizing how its components work together and their relevance to the optimisation process.

2.1 Model Overview

The model aims to describe the plasma temperature and confinement characteristics in a tokamak. It incorporates key physical processes such as energy deposition, current density, thermal transport, and power losses. The problem is formulated in a one-dimensional radial geometry, solving for the steady-state temperature profile $T(r)$ as a function of the radial coordinate r.

2.1.1 Formulating the Model

Energy Deposition Profiles: The plasma in a tokamak can be heated by external power sources to control the plasma. Two mechanisms—neutral beam injection (NBI) and electron cyclotron heating (ECH)—are the

dominant schemes, and the only plasma control inputs in this model. These processes are mathematically represented by Gaussian power deposition profiles, which describe the radial distribution of energy input:

$$S_{\text{NBI}}(r) = \frac{P_{\text{NBI}}}{\sqrt{2\pi}\sigma} \exp\left(-\frac{(r - r_{\text{center,NBI}})^2}{2\sigma^2}\right)\left[1 + k\frac{(r - r_{\text{center,NBI}})}{R}\right], \tag{2}$$

$$S_{\text{ECH}}(r) = \frac{P_{\text{ECH}}}{\sqrt{2\pi}\sigma} \exp\left(-\frac{(r - r_{\text{center,ECH}})^2}{2\sigma^2}\right), \tag{3}$$

where P_{NBI} and P_{ECH} are the total power injected by each mechanism, and σ defines the profile width [10, 11].

Toroidal Current and Ohmic Heating: In addition to the external inputs described in equations (1) and (2), the plasma generates internal energy through resistive heating caused by the toroidal current, modeled as a parabolic distribution:

$$j_\phi(r) = j_0\left(1 - \frac{r^2}{R^2}\right), \tag{4}$$

where j_0 is the peak current density. The resistive heating rate is given by:

$$S_{\text{Ohmic}}(r) = \eta j_\phi^2, \tag{5}$$

where η is the plasma resistivity, which depends on temperature [12].

Energy Transport and Losses: Radial energy transport occurs through thermal diffusivity. The effective thermal diffusivity, χ_{eff}, incorporates both neoclassical transport and turbulence. Turbulent transport depends on the local temperature gradient and energy deposition profiles:

$$\chi_{\text{eff}} = \chi_{\text{neo}} + \chi_0\left[\max\left(0, \frac{\frac{\partial T}{\partial r}}{T_{\text{crit,grad}}} - 1\right)\right]^\beta \cdot \tanh\left(S_{\text{ECH}} + S_{\text{NBI}}\right)^{\alpha_{\text{feedback}}}, \tag{6}$$

where χ_{neo} is the neoclassical diffusivity, and $T_{\text{crit,grad}}$ is the critical temperature gradient for turbulence onset [13, 14, 15].

Energy losses are modeled as radiative and convective processes [13]. Radiative losses are expressed as:

$$S_{\text{rad}}(r) = C_{\text{rad}} n_e^2 Z_{\text{eff}} \sqrt{T}, \tag{7}$$

where n_e is the electron density, Z_{eff} is the effective charge state, and C_{rad} is a proportionality constant. Convective losses introduce radial dependence:

$$S_{\text{conv}}(r) = \kappa_{\text{conv}}\left|\frac{\partial T}{\partial r}\right|\left(1 + 0.1\sin\left(\frac{2\pi r}{R}\right)\right). \tag{8}$$

Steady-State Power Balance: The steady-state temperature profile $T(r)$ satisfies the heat transport equation:

$$\frac{\chi_{\text{eff}}}{dr^2}\left(T_{i+1} - 2T_i + T_{i-1}\right) + \frac{S_{\text{total}}}{n_e c_e} - S_{\text{rad}} - S_{\text{conv}} = 0, \tag{9}$$

where the total source term S_{total} combines all contributions:

$$S_{\text{total}} = S_{\text{NBI}} + S_{\text{ECH}} + S_{\text{Ohmic}}. \tag{10}$$

This equation is solved iteratively on a discretized radial grid to obtain $T(r)$, from which other key parameters, such as the confinement time τ_E, are derived [16, 17].

Confinement Time: The energy confinement time τ_E quantifies how effectively the plasma retains energy and is defined as:

$$\tau_E = \frac{W}{P_{\text{total}}}, \tag{11}$$

where W, the stored energy, is:

$$W = \int 3 n_e T \cdot \text{keV\_to\_J} \cdot 2\pi r \, dr, \tag{12}$$

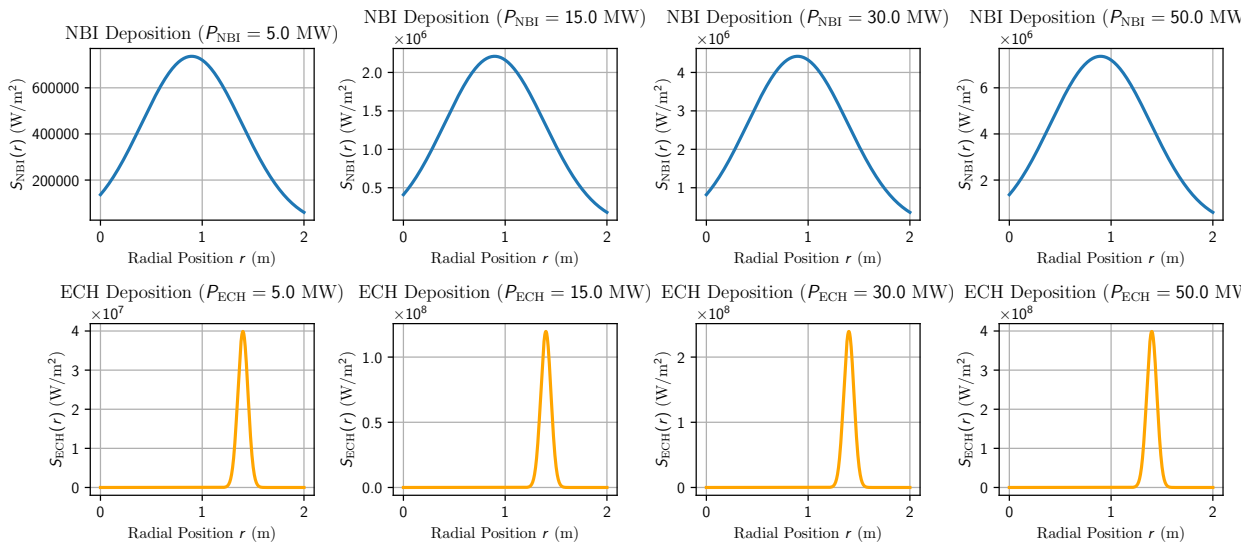

Figure 2: The calculated diagnostic parameters output from the model (to check physical relevance). The top figure shows the radial plasma temperature profile, and the bottom shows the radial current profile. The tokamak geometry is inspired by ITER, with plasma radius of 2 m, electron density of 1×10^{20}.

and P_{total}, the net power input, includes:

$$P_{\text{total}} = P_{\text{NBI}} + P_{\text{ECH}} + \int S_{\text{Ohmic}} \cdot 2\pi r \, dr - \int S_{\text{rad}} \cdot 2\pi r \, dr - \int S_{\text{conv}} \cdot 2\pi r \, dr. \tag{13}$$

This equation for τ_E represents the objective function in the later optimisation problem [13].

Stochastic Variation: Due to the simplistic nature of this model, random noise can be introduced to the base values of P_{NBI} and P_{ECH} to account for other affects that have not been included in the model [18]. This is expressed as:

$$P_{\text{varied}} = P_{\text{base}} + \mathcal{N}(0, \sigma^2), \tag{14}$$

where $\mathcal{N}(0, \sigma^2)$ represents Gaussian noise with mean 0 and standard deviation proportional to the amplitude of the base value:

$$\sigma = \text{amplitude} \times P_{\text{base}}. \tag{15}$$

2.1.2 Numerical Implementation and Model Output

The heat transport equation is solved numerically by discretizing the radial domain into a 1D grid. Finite-difference approximations are used to compute spatial derivatives. Starting with an initial guess for $T(r)$, the profile is iteratively updated until the maximum change between successive iterations falls below a convergence threshold.

The key physical parameters of interest here are the plasma current and temperature (to check that the model is reasonable), which are presented in Figure 2, and the confinement time. The confinement time is calculated for combinations of P_{NBI} and P_{ECH} from 0 to 50 MW each (for reference, ITER is using two NBI beams at 16.5 MW each and an array of ECH beams totaling 67 MW [19]). The resultant solution space, which will be optimised for in this investigation, can be seen in Figure 3.

2.2 Mathematical Optimisation

With the model constructed, and checked to be physically relevant, we can turn to the subject of optimisation. In this section, the choice of approach is discussed, and the implementation of the selected approach is detailed.

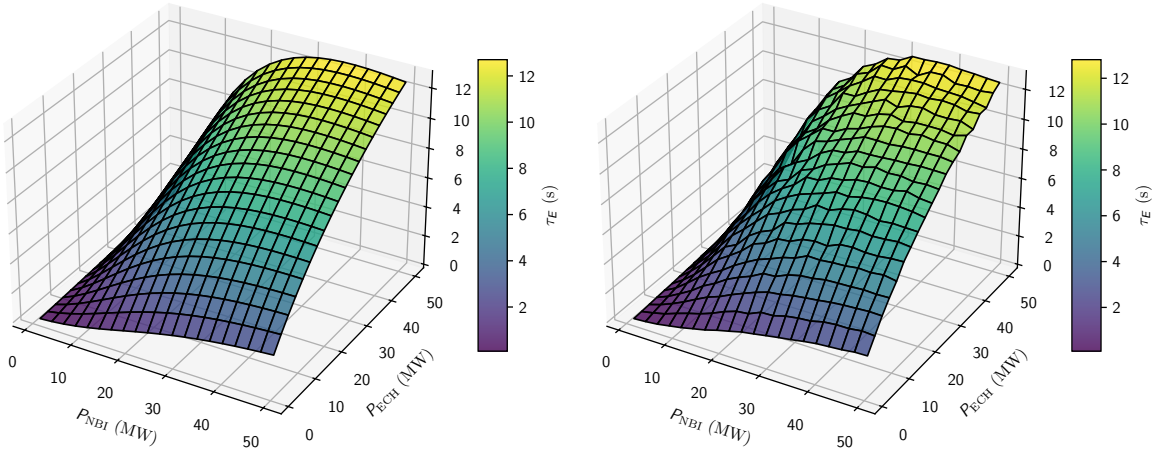

Figure 3: The solution space in τ_E that is the main result of the model and will later be optimised. The solution space is presented as the base output of the code (left), and with stochastic variation applied (right) to account for higher order effects not explicitly accounted for in the code.

2.2.1 Choice of Programming Approach

A range of optimisation approaches were considered and evaluated using the logic outlined in table 1. It was decided that owing to the non-convexity, stochasticity, and complexity of the solution space, simulated annealing was the most suitable optimisation approach.

Table 1: Decision-making process for selecting the optimisation technique.

Question	**Observation**	**Reasoning**	**Implication**
Is the problem linear or non-linear?	Non-linear objective function (see equations 11-13).	Linear techniques like Simplex cannot handle non-linearity.	Use a non-linear technique.
Is the model constrained or unconstrained?	Problem has constraints (see section 2.2.4).	Constraints require feasible solutions during optimization.	Use constrained optimisation techniques.
Is the solution space convex or non-convex?	Non-convex space (see Figure 3).	Non-convex spaces may trap local optima.	Use global or heuristic techniques.
Does the problem involve discrete or continuous variables?	Continuous variables, P_{NBI} and P_{ECH}.	Discrete techniques like integer programming are unnecessary.	Use continuous-variable methods.
Can the gradient of the objective function be calculated?	Gradient is impractical due to complexity.	Calculating gradients is computationally expensive.	Use gradient-free methods.
Is the problem deterministic or stochastic?	Problem involves stochastic variations.	Deterministic methods may miss random effects.	Use stochastic methods.
Is global optimisation required?	Multiple local optima in non-convex space.	Local search methods may fail.	Use global optimisation techniques.

Table 2: Decision making process for optimisation algorithm selection.

2.2.2 Simulated Annealing Algorithm

Simulated annealing is a probabilistic optimisation technique inspired by the annealing process in metallurgy, where a material is slowly cooled to minimize defects and achieve a stable crystalline structure [20, 21]. In this method, the solution space is explored by iteratively accepting new solutions, with the likelihood of accepting worse solutions decreasing over time, hence a 'cooling' effect. This balance of exploration and exploitation of promising solutions is particularly effective in irregular solution spaces where the algorithm can escape local minima [22].

1. **Initialization:**
   - Start with an initial solution $(P_{\text{NBI}}^{(0)}, P_{\text{ECH}}^{(0)})$.
   - Set the initial temperature T_0 and define the cooling schedule.
2. **Neighborhood Generation:**
   - Randomly perturb the current solution to generate a new candidate:

$$P'_{\text{NBI}} = \text{clip}(P_{\text{NBI}} + \Delta_{\text{NBI}}, 0, P_{\text{max, NBI}}),$$

$$P'_{\text{ECH}} = \text{clip}(P_{\text{ECH}} + \Delta_{\text{ECH}}, 0, P_{\text{max, ECH}}),$$

   where Δ_{NBI} and Δ_{ECH} are random perturbations.
3. **Acceptance Criterion:**
   - Compute the objective change:

$$\Delta f = f(P'_{\text{NBI}}, P'_{\text{ECH}}) - f(P_{\text{NBI}}, P_{\text{ECH}}).$$

- Accept the new candidate with probability:

$$P_{\text{accept}} = \begin{cases} 1, & \text{if } \Delta f > 0, \\ \exp\left(\frac{\Delta f}{T}\right), & \text{if } \Delta f \leq 0. \end{cases}$$

4. **Cooling Schedule:**

- Update the temperature:

$$T = T_0 \cdot \alpha^k,$$

where $\alpha \in (0, 1)$ is the cooling rate, and k is the current iteration.

The algorithm terminates when the maximum number of iterations $N_{\max}$ is reached.

2.2.3 Fine-tuning the optimisation

Within the framework of simulated annealing, various options are available to fine-tune the model, including the initial annealing temperature and the choice of cooling scheme [23]. In this study, we simultaneously explore the effects of these factors on model performance. Three cooling schemes were considered: exponential decay, logarithmic decay, and linear decay.

In the exponential decay scheme, the temperature decreases exponentially with the iteration number k, following the equation:

$$T(k) = T_0 \cdot \alpha^k, \tag{16}$$

where T_0 is the initial temperature, $\alpha \in (0, 1)$ is the cooling rate, and k is the current iteration.

Logarithmic decay, by contrast, reduces the temperature logarithmically as a function of k, according to:

$$T(k) = \frac{T_0}{\log(k + 2)}, \tag{17}$$

where T_0 is again the initial temperature, and the offset $+2$ ensures numerical stability at $k = 0$.

Finally, in the linear decay scheme, the temperature decreases linearly with the iteration number k, following the expression:

$$T(k) = T_0 \cdot \left(1 - \frac{k}{N_{\max}}\right), \tag{18}$$

where T_0 is the initial temperature, $N_{\max}$ is the maximum number of iterations, and k is the current iteration. In this scheme, the temperature decreases to zero at the final iteration [24].

After defining the cooling schemes, their respective were optimised hyperparameters to maximise the average confinement time τ_E. For each cooling scheme, statistics were calculated from a sample of 50 optimisation runs to ensure reliable comparisons.

2.2.4 Constraint Formulation

For the results of the model to be relevant in the real world, it is essential to impose constraints [25, 26]. The first constraint limits the power values to realistically implementable ranges, ensuring that the heating systems operate within their technical capacities. The second constraint focuses on the total cost of the heating systems, reflecting practical budgetary limits. Together, these constraints ensure that the tokamak's actuation system is both technically and economically viable.

The steady-state temperature profile $T(r)$, derived from the heat transport equation, governs the plasma's energy balance and is defined as:

$$\frac{\chi_{\text{eff}}}{dr^2}\left(T_{i+1} - 2T_i + T_{i-1}\right) + \frac{S_{\text{total}}}{n_e c_e} - S_{\text{rad}} - S_{\text{conv}} = 0. \tag{19}$$

Here, the total energy source term, S_{total}, includes contributions from all heating mechanisms:

$$S_{\text{total}} = S_{\text{NBI}} + S_{\text{ECH}} + S_{\text{Ohmic}}. \tag{20}$$

This physical constraint ensures the steady-state energy balance, maintaining the physical accuracy of the model.

In addition to physical constraints, the costs associated with the heating systems must be considered. For Neutral Beam Injection (NBI) and Electron Cyclotron Heating (ECH), costs scale linearly with their respective power inputs:

$$C_{\text{NBI}} = k_{\text{NBI}} \cdot P_{\text{NBI}}, \quad C_{\text{ECH}} = k_{\text{ECH}} \cdot P_{\text{ECH}}. \tag{21}$$

Here, $k_{\text{NBI}} = \$12.5\,\text{m/MW}$ and $k_{\text{ECH}} = \$7.5\,\text{m/MW}$ represent the cost per unit power for NBI and ECH, respectively. To ensure economic feasibility, the total cost of heating is constrained by a predefined budget B, set to \$0.5 billion in this study:

$$C_{\text{NBI}} + C_{\text{ECH}} \leq B. \tag{22}$$

This constraint introduces a trade-off between maximizing the energy confinement time τ_E and minimizing operational costs, a critical consideration in large-scale plasma experiments.

Finally, the power inputs for NBI and ECH are restricted by the operational capacities of the heating systems:

$$0 \leq P_{\text{NBI}} \leq P_{\text{max,NBI}}, \quad 0 \leq P_{\text{ECH}} \leq P_{\text{max,ECH}}. \tag{23}$$

For this study, the maximum allowable power for each system is assumed to be 50 MW. These constraints ensure that the optimisation remains within the technical limits of the experimental apparatus, avoiding overloading or inefficient power utilization.

3 Results

As described in section 2.2.3, the simulated annealing algorithm was applied to the 2D surface of τ_E solutions generated by the physics model. For each of the described cooling schemes, 50 optimisation runs were performed for each initial temperature for $T_i = [10, 100, 500, 1000]$ K and the average and standard deviation of the set plotted in figure 4a. For all simulation runs, 500 iterations are performed. The average and standard deviation for best-performing combination is plotted in figure 4b where the combination that produced the highest mean τ_E was , while the lowest standard deviation overall was . From this set, due to the balance of high mean and low standard deviation, exponential decay with $T_i = 10$ K is selected as the optimal combination,with μ_τ (s) σ_τ =.

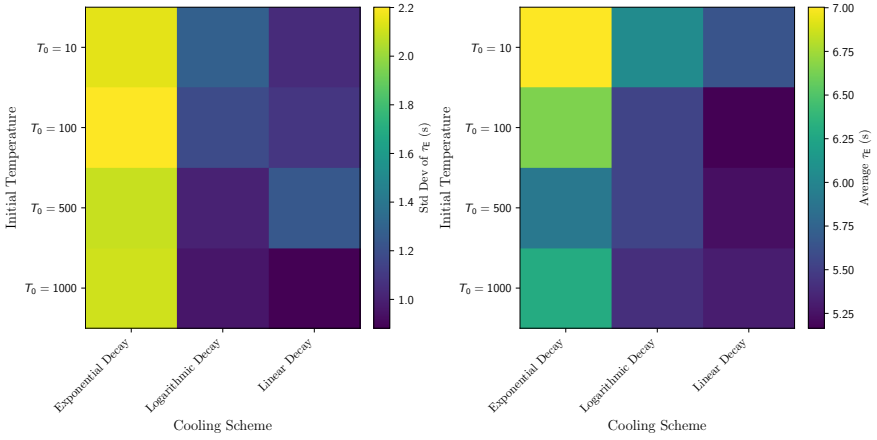

(a) Heatmaps of standard deviation (left) and average (right) τ_E across configurations.

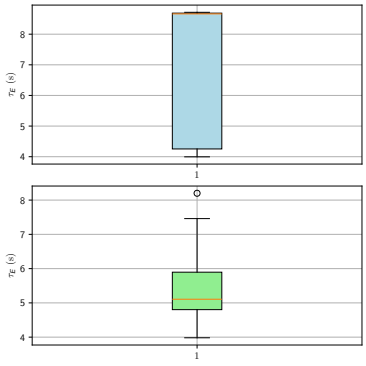

(b) Box plots of τ_E for highest mean (top) and lowest standard deviation (bottom) combinations. The top plot corresponds to $T_i = 10$ with exponential decay, and the bottom to $T_i = 1000$ with linear decay as the cooling scheme.

Figure 4: Comparison of heatmaps and box plots for simulated annealing results.

With the optimal T_i and cooling scheme combination determined, the value of α in equation 16 can be optimised. For $T_i = 10$ K, the average value of τ_E is plotted for α varying from 0.85 to 0.99. From figure 5 it can be seen that the optimal value is ~ 0.87. This value is used for all future optimisations.

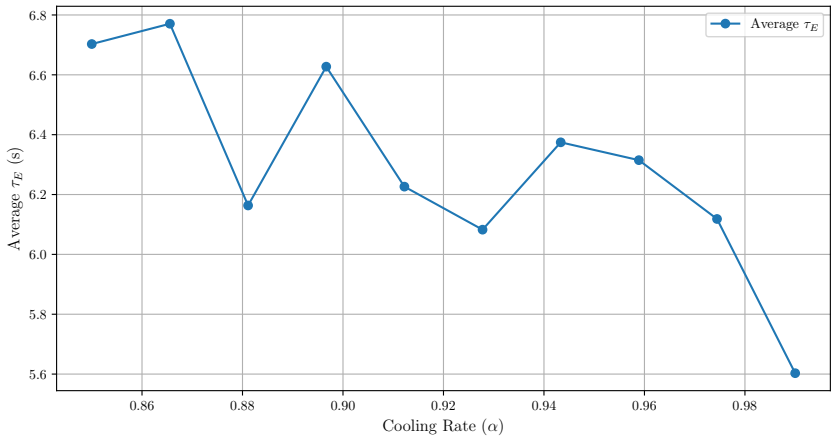

Figure 5: Effect of different values of α on τ_E (see equation 16), averaged over 50 runs each.

With this analysis completed, the final optimisation algorithm parameters were set as specified in table 3. For the non-stochastic solution space, the optimal value of τ_E was determined to be 8.712 s, where the full budget of \$500 million was used. For the stochastic solution space, the optimal value of τ_E was determined to be 8.605, where again, the full budget of \$500 million was used. The full results for both optimisations can be seen in table **??**.

Parameter	Value (stochastic)	Value (non-stochastic)
Initial temperature, T_i	100 K	100 K
Cooling scheme	Exponential decay ($\alpha = 0.87$)	Exponential decay ($\alpha = 0.87$)
Initial P_{NBI}	15 MW	15 MW
Initial P_{ECH}	15 MW	15 MW
Number of iterations	500	500
Max budget, B	\$0.5 billion USD	\$0.5 billion USD
k_{NBI}	\$12.5 million/MW	\$12.5 million/MW
k_{ECH}	\$7.5 million/MW	\$7.5 million/MW

Table 3: optimisation algorithm conditions for both stochastic and non-stochastic cases.

Parameter	Value (Non-Stochastic)	Value (Stochastic)
Optimal NBI Power	19.37 MW	23.71 MW
Optimal ECH Power	34.0 MW	26.65 MW
Maximum Confinement Time (τ_E)	8.712 s	8.605 s
Average Confinement Time (τ_E)	6.772 s	6.583 s
Cost of NBI	\$0.24 billion	\$0.30 billion
Cost of ECH	\$0.26 billion	\$0.20 billion
Total Cost	\$0.50 billion	\$0.50 billion

Table 4: optimisation results for both the stochastic and non-stochastic solution spaces (see Figure 3), using parameters as specified in Table 3.

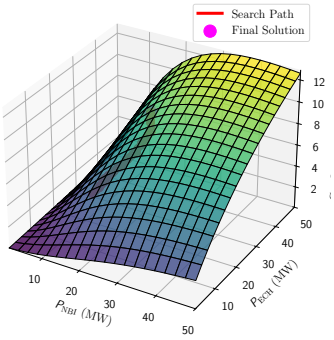

(a) Optimised 3D surface path for a non-stochastic solution space (500 iterations

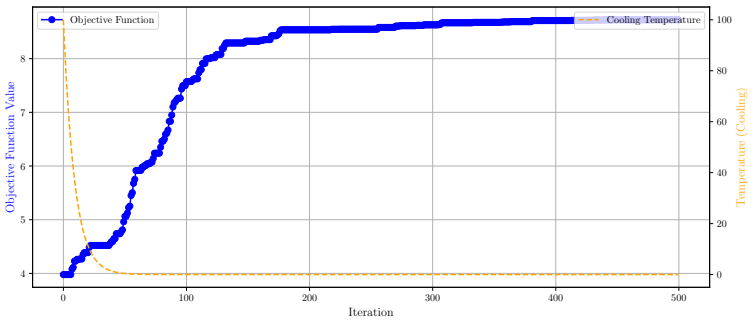

(b) Iteration path with temperature (exponential decay).

Figure 6: Comparison of the optimised 3D surface path and iteration path with temperature.

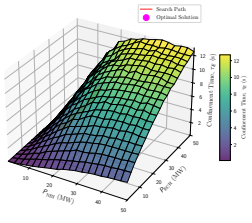

(a) Optimised 3D surface path for a stochastic solution space (500 iterations).

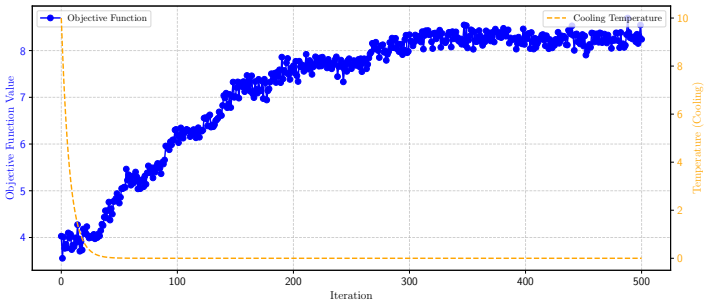

(b) Iteration path with temperature (exponential decay).

Figure 7: Comparison of the optimised 3D surface path and iteration path with temperature.

4 Discussion

The results of this study demonstrate the potential of simulated annealing coupled with a plasma model for providing valuable insights into decision making for fusion devices. This discussion details the successes and limitations of this approach.

The solution space for τ_E reveals notable physical insights. One might intuitively expect the global maximum of τ_E to occur at the maximum allowable actuation powers, $P_{\text{NBI}} = 50$ MW and $P_{\text{ECH}} = 50$ MW. However, as shown in Figures 3 and 4, this is not the case. Instead, as the plasma becomes saturated with input power, competing effects such as enhanced turbulence and transport losses (governed by equation 6) dominate, reducing τ_E beyond a critical threshold. Additionally, the absorption profiles (equation 3) demonstrate that the spatial distribution of energy deposition is highly localised, which further complicates the dependence of τ_E on input power.

For the non-stochastic case, the optimal configuration corresponds to $P_{\text{NBI}} = 19.37$ MW and $P_{\text{ECH}} = 34.0$ MW, resulting in an energy confinement time of $\tau_E = 8.712$ seconds while utilising the full budget of \$500 million. For the stochastic case, the optimal configuration is $P_{\text{NBI}} = 23.71$ MW and $P_{\text{ECH}} = 26.65$ MW, achieving $\tau_E = 8.605$ seconds, under the same budget constraint. The percentage difference in τ_E between the stochastic and non-stochastic cases is less than 2.83% (averaged over 50 runs each), indicating that despite the added complexity and presence of local minima in the stochastic solution space, the simulated annealing algorithm is capable of converging to near-optimal solutions in both cases.

Among the cooling schemes evaluated, exponential decay was the most effective, achieving the highest average τ_E and exhibiting the lowest standard deviation across trials. Specifically, the average τ_E for expo-

nential decay cooling was significantly higher compared to logarithmic and linear schemes, highlighting the importance of selecting an appropriate cooling strategy for non-convex, stochastic optimisation problems. Additionally, fine-tuning the cooling constant α revealed that the optimal value for this solution space was $\alpha = 0.87$, which is on the lower end of the usually recommended interval of 0.85-0.99, potentially highlighting the need for more exploration due to the nature of the solution space.

While this study demonstrates the potential of metaheuristic optimisation for tokamak control parameter tuning, there are several opportunities to enhance both the physical realism of the model and the effectiveness of the optimisation algorithm. From a modeling perspective, the one-dimensional plasma kinetics model provides a useful approximation but neglects several important physical processes. Incorporating magnetic field effects, such as inhomogeneities, ripple effects, and magnetic island dynamics, would improve the accuracy of the energy transport calculations. Similarly, edge-localised modes (ELMs) and scrape-off layer (SOL) physics could be modeled to better represent the plasma boundary, including sheath interactions and divertor energy flux. Anisotropic heat transport, which accounts for differences in parallel and perpendicular transport along magnetic field lines, could also provide a more realistic depiction of energy flow.

The optimisation algorithm itself could also benefit from enhancements. Coupling the simulated annealing approach with advanced transport codes, such as RAPTOR [27], could significantly improve the accuracy of the solution space by leveraging finite element methods for solving transport equations. This would provide a more detailed and physically representative basis for optimisation. Additionally, exploring adaptive cooling schedules, such as those proposed by Triki et al. [28], could improve convergence by dynamically adjusting the cooling rate based on the local solution landscape. Adaptive strategies provide more control over the annealing process and offer valuable insights into the quality of current equilibria and the complexity of the problem. Other numerical metaheuristic techniques, such as genetic algorithms or particle swarm optimization, could also be compared with simulated annealing to identify the most effective approach for this class of problems.

Despite these limitations, this study demonstrates the power of metaheuristics in tackling complex, non-linear optimisation problems in fusion energy research. By using simulated annealing, this work was able to identify optimal configurations of NBI and ECH actuation within technical and budgetary constraints, demonstrating that significant cost savings and performance improvements are possible. For example, by optimising actuation power allocation, potentially billions of dollars could be saved on large-scale tokamak systems, accelerating the development and deployment of fusion energy as a practical solution to the global energy and climate crisis.

In conclusion, this study demonstrates that combining a physics-based tokamak model with metaheuristic optimisation can effectively improve the performance of magnetic confinement fusion devices. By optimising costly systems like NBI and ECH, savings of potentially billions can be achieved, accelerating the development of economically viable fusion energy. Such advancements are essential for enabling fusion energy to contribute meaningfully to the transition to sustainable energy systems, helping to combat climate change and reduce reliance on fossil fuels.

References

[1] Carl-Friedrich Schleussner, Joeri Rogelj, Michiel Schaeffer, Tabea Lissner, Rachel Licker, Erich M Fischer, Reto Knutti, Anders Levermann, Katja Frieler, and William Hare. Science and policy characteristics of the paris agreement temperature goal. *Nature Climate Change*, 6(9):827–835, 2016.

[2] Richard SJ Tol. Costs and benefits of the paris climate targets. *arXiv preprint arXiv:2209.00900*, 2022.

[3] Culham Centre for Fusion Energy (CCFE). Joint european torus (jet), 2025. Accessed: 2025-01-24.

[4] S Woodruff. An overview of tokamak alternatives in the us fusion program with the aim of fostering concept innovation. *Journal of fusion energy*, 23(1):27–40, 2004.

[5] Stephen O Dean. Historical perspective on the united states fusion program. *Fusion science and technology*, 47(3):291–299, 2005.

[6] The Fusion Industry Association. The fusion industry supply chain: Opportunities and challenges, 2023.

[7] John D Lawson. Some criteria for a power producing thermonuclear reactor. *Proceedings of the physical society. Section B*, 70(1):6, 1957.

[8] Samuel E Wurzel and Scott C Hsu. Progress toward fusion energy breakeven and gain as measured against the lawson criterion. *Physics of Plasmas*, 29(6), 2022.

[9] *Considerations of Technology Readiness Levels for Fusion Technology Components*. Number 2047 in TECDOC Series. INTERNATIONAL ATOMIC ENERGY AGENCY, Vienna, 2024.

[10] Robert J Goldston, DC McCune, HH Towner, SL Davis, RJ Hawryluk, and GL Schmidt. New techniques for calculating heat and particle source rates due to neutral beam injection in axisymmetric tokamaks. *Journal of computational physics*, 43(1):61–78, 1981.

[11] V Erckmann and U Gasparino. Electron cyclotron resonance heating and current drive in toroidal fusion plasmas. *Plasma physics and controlled fusion*, 36(12):1869, 1994.

[12] Jeffrey P Freidberg. *Plasma physics and fusion energy*. Cambridge university press, 2008.

[13] Francis F Chen et al. *Introduction to plasma physics and controlled fusion*, volume 1. Springer, 1984.

[14] Radu Balescu. Transport processes in plasmas. classical transport theory. vol. 1. 1988.

[15] FL Hinton and Richard D Hazeltine. Theory of plasma transport in toroidal confinement systems. *Reviews of Modern Physics*, 48(2):239, 1976.

[16] Archie A Harms, Dave R Kingdon, George H Miley, and Klaus F Schoepf. *Principles of fusion energy: an introduction to fusion energy for students of science and engineering*. World Scientific Publishing Company, 2000.

[17] Weston M Stacey. *Fusion plasma physics*. John Wiley & Sons, 2012.

[18] Setsuo Ichimaru. *Statistical plasma physics, volume I: basic principles*. CRC Press, 2018.

[19] ITER Organization. External heating systems, 2024. Accessed: 2024-12-30.

[20] Alex Kwaku Peprah, Simon Kojo Appiah, Samuel Kwame Amponsah, et al. An optimal cooling schedule using a simulated annealing based approach. *Applied Mathematics*, 8(08):1195, 2017.

[21] Peter JM Van Laarhoven, Emile HL Aarts, Peter JM van Laarhoven, and Emile HL Aarts. *Simulated annealing*. Springer, 1987.

[22] Thomas Guilmeau, Emilie Chouzenoux, and Víctor Elvira. Simulated annealing: A review and a new scheme. In *2021 IEEE statistical signal processing workshop (SSP)*, pages 101–105. IEEE, 2021.

[23] Harry Cohn and Mark Fielding. Simulated annealing: searching for an optimal temperature schedule. *SIAM Journal on Optimization*, 9(3):779–802, 1999.

[24] Jonathan Thompson and Kathryn A Dowsland. General cooling schedules for a simulated annealing based timetabling system. In *Practice and Theory of Automated Timetabling: First International Conference Edinburgh, UK, August 29–September 1, 1995 Selected Papers 1*, pages 345–363. Springer, 1996.

[25] JW Van Groenigen and A Stein. Constrained optimization of spatial sampling using continuous simulated annealing. Technical report, Wiley Online Library, 1998.

[26] H Edwin Romeijn and Robert L Smith. Simulated annealing for constrained global optimization. *Journal of Global Optimization*, 5:101–126, 1994.

[27] J Van Dongen, F Felici, GMD Hogeweij, P Geelen, and E Maljaars. Numerical optimization of actuator trajectories for iter hybrid scenario profile evolution. *Plasma Physics and Controlled Fusion*, 56(12):125008, 2014.

[28] Eric Triki, Yann Collette, and Patrick Siarry. A theoretical study on the behavior of simulated annealing leading to a new cooling schedule. *European Journal of Operational Research*, 166(1):77–92, 2005.